Impedance-based analysis of HVDC converter control for robust stability in AC power systems

André Schön, Andreas Lorenz, Rodrigo Alonso Alvarez Valenzuela
SIEMENS ENERGY GLOBAL GMBH & CO. KG
schoen.andre@siemens-energy.com

Keywords
≪Converter control≫, ≪HVDC≫, ≪MMC≫, ≪Impedance analysis≫, ≪Stability≫

Abstract
Ensuring robust control stability to varying grid conditions is a key requirement when installing a new HVDC station to the AC grid. With its very accessible criteria for stability margins, the Nyquist theorem for single input/single output systems is commonly used to determine the robustness of the control system of HVDC converter stations and tune it accordingly. However, three-phase AC system are not single input/single output systems and the validity as well as the underlying assumptions of this investigation has rarely been under scrutiny. In this paper, the commonly used impedance based approach to assess stability and robustness of HVDC converter stations is reviewed from a control theoretical point of view. Starting with a clarification on the properties of commonly used reference system transformations, the repercussions for robustness investigations in a multivariable control environment are discussed. Based on that, possible shortcuts to allow classical single input/single output investigations as well as limitations to that approach are derived and explained in detail on a generic control model.

1 Introduction
AC power systems with a high penetration of power electronic (PE), actively controlled components face new challenges assessing the overall system stability. The impedance based analysis of AC power systems offers a comprehensive approach, where each component of the grid is modelled by its terminal behavior. Each subsystem can be described as an independent black box, with no necessary information on the internal physical or electrical structure. These models can be determined by analytical calculations or even by frequency sweep measurements[1–9]. Interactions of PE devices with the grid and with each other can then be investigated from a top level perspective.

The general requirements for PE components are primarily given by specific control goals for the stationary operation and dynamic requirements, like the fault ride through behavior or specific step responses. To avoid harmful interactions, the requirements to the frequency domain input impedance often include positive damping for a very wide frequency range and even certain phase margins or adjustable damping in specific frequency areas with the goal of ensuring robust, stable operation for unknown and varying grid conditions [10–12].

In this paper, the validity of the commonly used approach, to investigate stability and control robustness based solely on the main diagonal elements of the converter input admittance (e.g. [5–7, 13–15]) is dissected. With the help of control theoretical concepts for multi variable feedback systems, boundary conditions to the calculation method and to the grid conditions for the validity of this approach are derived.

In Section 2 the general approach for an analytical description of the converter input impedance as well as its challenges are outlined based on a generic control structure. Section 3 reviews common reference systems for the description of the converter input impedance and their (dis)advantages. Section 4 reviews the stability problem from a control theoretical perspective and shows possible shortcuts based on an advantageous reference system selection and boundaries to the grid impedance. Section 5 combines the

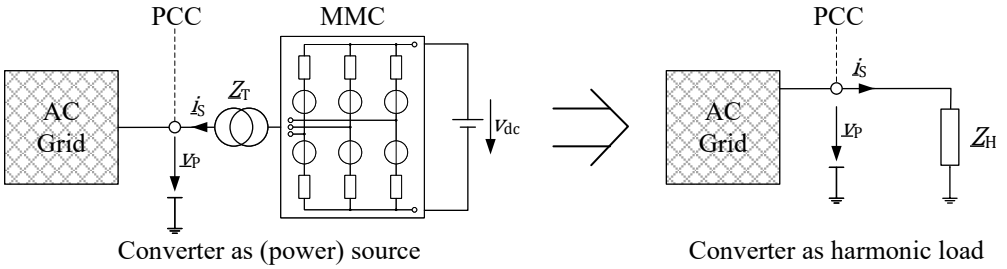

Fig. 1: Impedance based analysis - the source converter is modelled as a harmonic load to the grid

results of the previous sections into an evaluation of an exemplary converter system and describes the conditions for a classical stability analysis as well as the relations between the converter input impedance and the performance requirements of the converter.

2 Calculation of the converter input impedance

From a control perspective, any perturbation in the voltage at the point of common coupling (PCC) is a disturbance to the stationary control targets of the converter control. Any voltage perturbation leads to a corresponding response in the line current due to the internal control. To evaluate the feedback effects between an AC grid and a converter station, the converter is modelled as a harmonic load at the PCC (see Fig. 1). Since HVDC converter station transformers usually decouple the zero sequence, any zero sequence interaction between converter and AC grid is limited to parasitic effects which, for the sake of clarity, are neglected here. Hence, for this paper, any 3-by-3 AC impedances matrix is reduced to a 2-by-2 matrix. The analysis will only be shown in the αβ and the *dq* frame as well as in the sequence domain (*PN*). Whenever a specific reference frame is regarded, the variables will be denoted with the indices αβ, *dq* or *PN*. Variables without denotation regard to any reference frame.

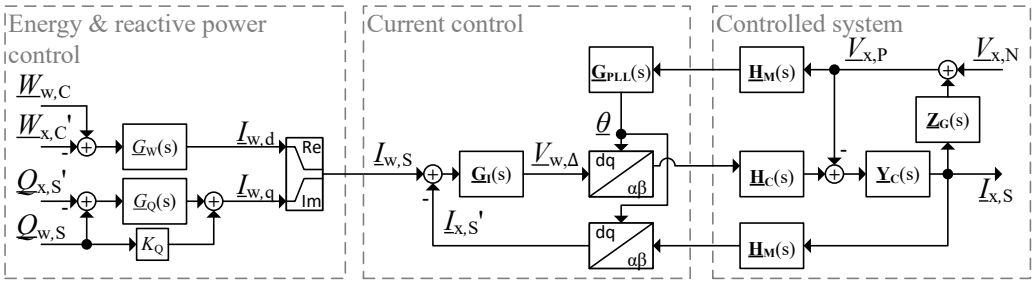

Fig. 2: Generalized MMC control diagram

In general, there are two options to model the converter input impedance. One option is to calculate the disturbance response of the converter control analytically, the other option is to measure the input impedance directly via a voltage (or current) perturbation frequency sweep directly at the PCC in a simulation model or if possible, given the physical limitations, at the real device. Analytical approaches often face difficulties with non-linearities or with selecting the right reference frame. They also often lead to models with a very high order, especially when dead times are involved, which can increase the computational time drastically. Measured models on the other hand lead to reduced accuracy and tend to neglect narrow banded effects depending on the frequency resolution of the measurement sweep. They are not generally suited for stability analysis, can however validate analytical models. Fig. 2 shows a generalized control model [9, 15–17] including an inner current controller $\underline{\mathbf{G}}_I$ and energy as well as a reactive power controller $\underline{\mathbf{G}}_{WQ}$ forming secondary control layers. The controlled electrical system is divided into a summarized grid impedance $\underline{\mathbf{Z}}_G$ and the electrical components of to converter station up to the PCC $\underline{\mathbf{Y}}_C$, containing e.g. the converter transformer and the arm impedances. The model also contains a PLL $\underline{\mathbf{G}}_{PLL}$ and a measurement system $\underline{\mathbf{H}}_M$ including dead times. The generation of the physical output voltage is combined in $\underline{\mathbf{H}}_C$. Due to the high number of voltage levels and the resulting high effective switching frequency in each converter arm, for Modular Multilevel Converters (MMC) in an HVDC application, the output voltage can be modelled as a delayed ideal voltage source. Due to the

non-linearities, the linearized small signal converter model is highly operation point dependent. For the simplified control structure of Fig. 2, the input impedance calculates to

$$\underline{\mathbf{Y}}_{\mathrm{H}} = -\frac{\vec{\underline{I}}_{\mathrm{x,S}}}{\vec{\underline{V}}_{\mathrm{x,P}}} = \left(\mathbf{I}+\underline{\mathbf{Y}}_{\mathrm{C}}\underline{\mathbf{H}}_{\mathrm{C}}\underline{\mathbf{G}}_{\mathrm{I}}\left(\mathbf{I}+\tfrac{3}{2}\underline{\mathbf{G}}_{\mathrm{WQ}}\underline{\mathbf{V}}_{\mathrm{P0}}\right)\underline{\mathbf{H}}_{\mathrm{M}}\right)^{-1}\cdot\underline{\mathbf{Y}}_{\mathrm{C}}\left(\mathbf{I}+\underline{\mathbf{H}}_{\mathrm{C}}\left(\left(\underline{\mathbf{G}}_{\mathrm{I}}\underline{\mathbf{I}}_{\mathrm{Sm,0}}-\underline{\mathbf{V}}_{\Delta,0}\right)\underline{\mathbf{G}}_{\mathrm{PLL}}+\tfrac{3}{2}\underline{\mathbf{G}}_{\mathrm{I}}\underline{\mathbf{G}}_{\mathrm{WQ}}\underline{\mathbf{I}}_{\mathrm{S},0}\right)\underline{\mathbf{H}}_{\mathrm{M}}\right) \quad (1)$$

with the voltage and current operation point

$$\underline{\mathbf{I}}_{\mathrm{Sm,0}}=\begin{bmatrix}\underline{I}_{\mathrm{Sm,d0}} & \underline{I}_{\mathrm{Sm,q0}}\\ \underline{I}_{\mathrm{Sm,q0}} & -\underline{I}_{\mathrm{Sm,d0}}\end{bmatrix},\ \underline{\mathbf{I}}_{\mathrm{S,0}}=\begin{bmatrix}\underline{I}_{\mathrm{S,d0}} & \underline{I}_{\mathrm{S,q0}}\\ -\underline{I}_{\mathrm{S,q0}} & \underline{I}_{\mathrm{S,d0}}\end{bmatrix},\ \underline{\mathbf{V}}_{\Delta,0}=\begin{bmatrix}\underline{V}_{\Delta,\mathrm{d0}} & -\underline{V}_{\Delta,\mathrm{q0}}\\ \underline{V}_{\Delta,\mathrm{q0}} & \underline{V}_{\Delta,\mathrm{d0}}\end{bmatrix}\text{ and }\underline{\mathbf{V}}_{\mathrm{P},0}=\begin{bmatrix}\underline{V}_{\mathrm{P,d0}} & \underline{V}_{\mathrm{P,q0}}\\ \underline{V}_{\mathrm{P,q0}} & -\underline{V}_{\mathrm{P,d0}}\end{bmatrix}.$$

The generic control structure, shown in Fig. 2 has only three main control loops, energy respectively reactive power and AC current. The AC current controller bandwidth is up to 30 Hz, the energy controller bandwidth up to 10 Hz, which is also the frequency range, where the PLL is active and the reactive power controller is designed slow with up to 1 Hz bandwidth. Hardware design was chosen to operate at a maximum power of 800 MW as an example, which is also the operation point (rectifier) shown in Fig. 5. The assumed dead times are approximated 200 μs in the current controller loop. This configuration as well as the control structure given in Fig. 2 serve just as a generic example to facilitate the investigations of the following sections. The specific implementation and parametrization are of no concern to the understanding of this paper.

3 Reference System Selection — αβ, *dq* and *PN*

In this section we investigate the I/O map of linear systems under commonly used signal transformations. A linear I/O map can be described through a transfer function matrix (TFM) in the Laplace domain, denoted by $\underline{\mathbf{G}}(\mathrm{s})$ which maps the input signal $\vec{\underline{u}}(t) \circ\!\!-\!\!\bullet\, \vec{\underline{U}}(\mathrm{s})$ to the output signal $\vec{\underline{y}}(t) \circ\!\!-\!\!\bullet\, \vec{\underline{Y}}(\mathrm{s})$. Application of a regular linear coordinate transformation $\underline{\mathbf{T}}(t) \in \mathbb{C}^{n\times n}$ to the in- and output signals then result in

$$\vec{\underline{y}} = \underline{\mathbf{T}}^{-1}\cdot\mathcal{L}^{-1}\left\{\underline{\mathbf{G}}\cdot\mathcal{L}\{\underline{\mathbf{T}}\cdot\vec{\underline{u}}\}\right\} \quad (2)$$

The transformed I/O map given by Eq.(2) is in general no longer a linear map and therefore cannot be described by a TFM in the Laplace domain. However, for the special case of a constant transformation matrix $\underline{\mathbf{T}}$ Eq.(2) becomes $\vec{\underline{Y}} = \underline{\mathbf{T}}^{-1}\underline{\mathbf{G}}\underline{\mathbf{T}}\cdot\vec{\underline{U}}$ and the coordinate transformation induces the transformation

$$\tilde{\underline{\mathbf{G}}} := \underline{\mathbf{T}}^{-1}\underline{\mathbf{G}}\underline{\mathbf{T}} \ \leftrightarrow \underline{\mathbf{G}} = \underline{\mathbf{T}}\tilde{\underline{\mathbf{G}}}\underline{\mathbf{T}}^{-1} \quad (3)$$

for the TFM, which immediately implies that the new I/O map is again linear with the new structure $\tilde{\underline{\mathbf{G}}}$. This transformation does not change the eigenvalues of the I/O map [18]. These preliminaries and notations now enable us to describe the influence of often used signal transformations to the I/O map of linear systems.

3.1 Input/Output map under *PN* transformation

The PN transformation, which associates real signals with complex signals in the time domain, is a constant, linear, complex signal transformation and therefore induces a transformation to the TFM given by Eq.(3):

$$\underline{\mathbf{G}}_{\mathrm{PN}} = \overbrace{\frac{1}{2}\begin{bmatrix}1 & \mathrm{j}\\ 1 & -\mathrm{j}\end{bmatrix}}^{\underline{\mathbf{T}}_{\mathrm{PN}}}\begin{bmatrix}\underline{G}_{11} & \underline{G}_{12}\\ \underline{G}_{21} & \underline{G}_{22}\end{bmatrix}\overbrace{\begin{bmatrix}1 & 1\\ -\mathrm{j} & \mathrm{j}\end{bmatrix}}^{\underline{\mathbf{T}}_{\mathrm{PN}}^{-1}} = \frac{1}{2}\begin{bmatrix}\underline{G}_{11}+\underline{G}_{22}-\mathrm{j}(\underline{G}_{12}-\underline{G}_{21}) & \underline{G}_{11}-\underline{G}_{22}+\mathrm{j}(\underline{G}_{12}+\underline{G}_{21})\\ \underline{G}_{11}-\underline{G}_{22}-\mathrm{j}(\underline{G}_{12}+\underline{G}_{21}) & \underline{G}_{11}+\underline{G}_{22}+\mathrm{j}(\underline{G}_{12}-\underline{G}_{21})\end{bmatrix} \quad (4)$$

$$\underline{\mathbf{G}} = \frac{1}{2}\begin{bmatrix}1 & 1\\ -\mathrm{j} & \mathrm{j}\end{bmatrix}\begin{bmatrix}\underline{G}_{\mathrm{PP}} & \underline{G}_{\mathrm{PN}}\\ \underline{G}_{\mathrm{NP}} & \underline{G}_{\mathrm{NN}}\end{bmatrix}\begin{bmatrix}1 & \mathrm{j}\\ 1 & -\mathrm{j}\end{bmatrix} = \frac{1}{2}\begin{bmatrix}\underline{G}_{\mathrm{NN}}+\underline{G}_{\mathrm{NP}}+\underline{G}_{\mathrm{PN}}+\underline{G}_{\mathrm{PP}} & \mathrm{j}\,(\underline{G}_{\mathrm{PP}}+\underline{G}_{\mathrm{NP}}-\underline{G}_{\mathrm{PN}}-\underline{G}_{\mathrm{NN}})\\ \mathrm{j}\,(\underline{G}_{\mathrm{NN}}+\underline{G}_{\mathrm{NP}}-\underline{G}_{\mathrm{PN}}-\underline{G}_{\mathrm{PP}}) & \underline{G}_{\mathrm{NN}}-\underline{G}_{\mathrm{NP}}-\underline{G}_{\mathrm{PN}}+\underline{G}_{\mathrm{PP}}\end{bmatrix} \quad (5)$$

P and *N* stand for the positive phase sequence (PPS) and the negative phase sequence (NPS) which is a well known transformation [19], especially in the αβ frame. Nevertheless, *PN* transformation can be used on any 2-by-2 TFM. If the scalar transfer functions (TF) $\underline{G}_{ij}$ are conjugate symmetrical ($\underline{G}_{ij}(\mathrm{s}^*) = \underline{G}^*_{ij}(\mathrm{s})$ $\Leftrightarrow$ Laplace transforms of real signals), then the scalar TF in $\underline{\mathbf{G}}_{\mathrm{PN}}$ have complex coefficients, and therefore the conjugate symmetry in the Laplace domain is lost. But then these TF fulfill $\underline{G}_{\mathrm{PN}}(\mathrm{s}) = \underline{G}^*_{\mathrm{NP}}(\mathrm{s}^*)$ and $\underline{G}_{\mathrm{PP}}(\mathrm{s}) = \underline{G}^*_{\mathrm{NN}}(\mathrm{s}^*)$, which can be easily verified by direct computation from Eq.(4).

3.2 Input/Output map under Park transformation

The Park transformation from the αβ to the *dq* reference frame is a multiplication in the time domain with a rotation matrix $\mathbf{T}_\mathrm{P}$ to rotate the input vector by a time varying angle θ. Therefore, it changes the I/O map of the system as described by Eq.(2). By careful application of the Laplace transformation rules to Eq.(2), like e.g. stated in [20], it can be seen that the transformed I/O map only remains linear, if the TFM $\underline{\mathbf{G}}$ has the following structure:

$$\underline{\mathbf{G}} = \begin{bmatrix} \underline{G}_\mathrm{M} & \underline{G}_\mathrm{O} \\ -\underline{G}_\mathrm{O} & \underline{G}_\mathrm{M} \end{bmatrix} \text{ with } \mathbf{T}_\mathrm{P} = \begin{bmatrix} \cos\theta(t) & \sin\theta(t) \\ -\sin\theta(t) & \cos\theta(t) \end{bmatrix} \text{ and } \mathbf{T}_\mathrm{P}^{-1} = \begin{bmatrix} \cos\theta(t) & -\sin\theta(t) \\ \sin\theta(t) & \cos\theta(t) \end{bmatrix} \tag{6}$$

The resulting map between in and output signals given by Eq.(3) can be described by the induced TFM $\underline{\mathbf{G}}_\mathrm{dq}$ or $\underline{\mathbf{G}}_{\alpha\beta}$ of the form:

$$\alpha\beta \to dq:\ \underline{\mathbf{G}}_\mathrm{dq} = \begin{bmatrix} \underline{G}_\mathrm{M}^\mathrm{r} - \underline{G}_\mathrm{O}^\mathrm{i} & \underline{G}_\mathrm{M}^\mathrm{i} + \underline{G}_\mathrm{O}^\mathrm{r} \\ -\underline{G}_\mathrm{M}^\mathrm{i} - \underline{G}_\mathrm{O}^\mathrm{r} & \underline{G}_\mathrm{M}^\mathrm{r} - \underline{G}_\mathrm{O}^\mathrm{i} \end{bmatrix} \text{ and } dq \to \alpha\beta:\ \underline{\mathbf{G}}_{\alpha\beta} = \begin{bmatrix} \underline{G}_\mathrm{M}^\mathrm{r} + \underline{G}_\mathrm{O}^\mathrm{i} & -\underline{G}_\mathrm{M}^\mathrm{i} + \underline{G}_\mathrm{O}^\mathrm{r} \\ \underline{G}_\mathrm{M}^\mathrm{i} - \underline{G}_\mathrm{O}^\mathrm{r} & \underline{G}_\mathrm{M}^\mathrm{r} + \underline{G}_\mathrm{O}^\mathrm{i} \end{bmatrix} \tag{7}$$

$$\text{with} \quad \underline{G}_x^\mathrm{r} = \frac{1}{2}\left(\underline{G}_x(\mathrm{s}+\mathrm{j}\omega_0) + \underline{G}_x(\mathrm{s}-\mathrm{j}\omega_0)\right) \qquad \text{and} \qquad \underline{G}_x^\mathrm{i} = \frac{\mathrm{j}}{2}\left(\underline{G}_x(\mathrm{s}+\mathrm{j}\omega_0) - \underline{G}_x(\mathrm{s}-\mathrm{j}\omega_0)\right)$$

3.3 Input/Output map under combined Park and *PN* transformation

Section 3.1 shows that the *PN* transformation maintains the LTI system property and Section 3.2 shows under which conditions the Park transformation applied to real time domain signals maintains the linear I/O map. Now we investigate the change of the I/O map if the Park-transformation is applied to complex valued time domain signal in *PN* coordinates. From Eq.(2) and successive application of the signal transformation it can be obtained:

$$\alpha\beta_\mathrm{PN} \to dq_\mathrm{PN}:\ \vec{\underline{y}}_\mathrm{PN}^\mathrm{dq} = \underline{\mathbf{T}}_\mathrm{PN}\mathbf{T}_\mathrm{P}(t)\underline{\mathbf{T}}_\mathrm{PN}^{-1} \cdot \mathcal{L}^{-1}\{\underline{\mathbf{G}}_\mathrm{PN}^{\alpha\beta}(\mathrm{s}) \cdot \mathcal{L}\{\underline{\mathbf{T}}_\mathrm{PN}\mathbf{T}_\mathrm{P}^{-1}(t)\underline{\mathbf{T}}_\mathrm{PN}^{-1} \cdot \vec{\underline{u}}_\mathrm{PN}^\mathrm{dq}(t)\}\} \tag{8}$$

$$dq_\mathrm{PN} \to \alpha\beta_\mathrm{PN}:\ \vec{\underline{y}}_\mathrm{PN}^{\alpha\beta} = \underline{\mathbf{T}}_\mathrm{PN}\mathbf{T}_\mathrm{P}^{-1}(t)\underline{\mathbf{T}}_\mathrm{PN}^{-1} \cdot \mathcal{L}^{-1}\{\underline{\mathbf{G}}_\mathrm{PN}^\mathrm{dq}(\mathrm{s}) \cdot \mathcal{L}\{\underline{\mathbf{T}}_\mathrm{PN}\mathbf{T}_\mathrm{P}(t)\underline{\mathbf{T}}_\mathrm{PN}^{-1} \cdot \vec{\underline{u}}_\mathrm{PN}^{\alpha\beta}(t)\}\} \tag{9}$$

$$\text{with } \underline{\mathbf{T}}_\mathrm{PN}\mathbf{T}_\mathrm{P}^{-1}(t)\underline{\mathbf{T}}_\mathrm{PN}^{-1} = \begin{bmatrix} \mathrm{e}^{\mathrm{j}\omega_0 t} & 0 \\ 0 & \mathrm{e}^{-\mathrm{j}\omega_0 t} \end{bmatrix} \text{ and } \underline{\mathbf{T}}_\mathrm{PN}\mathbf{T}_\mathrm{P}(t)\underline{\mathbf{T}}_\mathrm{PN}^{-1} = \begin{bmatrix} \mathrm{e}^{-\mathrm{j}\omega_0 t} & 0 \\ 0 & \mathrm{e}^{\mathrm{j}\omega_0 t} \end{bmatrix}$$

$$\begin{aligned} \vec{\underline{Y}}_\mathrm{PN}^\mathrm{dq} = &\begin{bmatrix} \underline{G}_\mathrm{PP}^{\alpha\beta}(\mathrm{s}+\mathrm{j}\omega_0) & 0 \\ 0 & \underline{G}_\mathrm{NN}^{\alpha\beta}(\mathrm{s}-\mathrm{j}\omega_0) \end{bmatrix} \begin{bmatrix} \underline{U}_\mathrm{P}^\mathrm{dq}(\mathrm{s}) \\ \underline{U}_\mathrm{N}^\mathrm{dq}(\mathrm{s}) \end{bmatrix} \\ &+ \begin{bmatrix} 0 & \underline{G}_\mathrm{PN}^{\alpha\beta}(\mathrm{s}+\mathrm{j}\omega_0) \\ \underline{G}_\mathrm{NP}^{\alpha\beta}(\mathrm{s}-\mathrm{j}\omega_0) & 0 \end{bmatrix} \begin{bmatrix} \underline{U}_\mathrm{P}^\mathrm{dq}(\mathrm{s}-\mathrm{j}2\omega_0 t) \\ \underline{U}_\mathrm{N}^\mathrm{dq}(\mathrm{s}+\mathrm{j}2\omega_0 t) \end{bmatrix} \end{aligned} \tag{10}$$

$$\begin{aligned} \vec{\underline{Y}}_\mathrm{PN}^{\alpha\beta} = &\begin{bmatrix} \underline{G}_\mathrm{PP}^\mathrm{dq}(\mathrm{s}-\mathrm{j}\omega_0) & 0 \\ 0 & \underline{G}_\mathrm{NN}^\mathrm{dq}(\mathrm{s}+\mathrm{j}\omega_0) \end{bmatrix} \begin{bmatrix} \underline{U}_\mathrm{P}^{\alpha\beta}(\mathrm{s}) \\ \underline{U}_\mathrm{N}^{\alpha\beta}(\mathrm{s}) \end{bmatrix} \\ &+ \begin{bmatrix} 0 & \underline{G}_\mathrm{PN}^\mathrm{dq}(\mathrm{s}-\mathrm{j}\omega_0) \\ \underline{G}_\mathrm{NP}^\mathrm{dq}(\mathrm{s}+\mathrm{j}\omega_0) & 0 \end{bmatrix} \begin{bmatrix} \underline{U}_\mathrm{P}^{\alpha\beta}(\mathrm{s}+\mathrm{j}2\omega_0 t) \\ \underline{U}_\mathrm{N}^{\alpha\beta}(\mathrm{s}-\mathrm{j}2\omega_0 t) \end{bmatrix} \end{aligned} \tag{11}$$

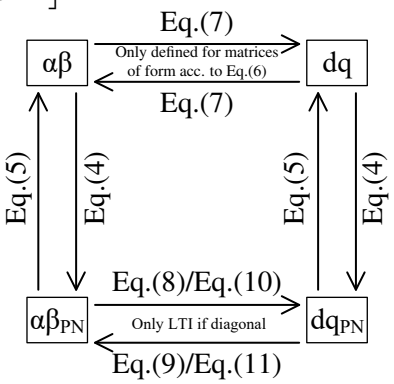

Fig. 3: Commutative graph for transfer function matrix transformation between αβ, *dq* and *PN* frame

Evaluation of Eq.(10) and Eq.(11) reveals that the I/O map of the system has to be diagonal to maintain the LTI property because off-diagonal elements of $\underline{\mathbf{G}}_\mathrm{PN}$ lead to system responses at shifted frequencies compared to the input signal $\vec{\underline{u}}$. Eq.(4) to Eq.(11) build a commutative diagram of successive signal transformations and ensure that the coordinates can be switched for a convenient system description (compare to e.g. [1, 5, 8, 9, 18, 21–23]).

4 Impedance based stability analysis and requirements to the grid impedance

This chapter, relates the established impedance-based stability analysis to the well-known control theoretical concepts of passivity and the small gain theorem. These concepts are introduced by using of the Nyquist theorem, beginning with the SISO case. Also, the necessity to extend these stability analysis methods to the MIMO system case for HVDC applications will be motivated and the obstacles that arise thereby will be pointed out. Finally, a direct Nyquist array method to reduce the MIMO case to multiple SISO systems is utilized, circumventing the problems described and restoring the benefits of standard control design methods in the frequency domain for the MIMO case.

4.1 Control theoretical interpretation of the stability problem in electrical systems

The general control representation of the converter grid interconnection at a PCC is given in Fig. 4 [4, 17]. The converter station is represented by its input admittance $\underline{\mathbf{Y}}_{\mathrm{H}}$ and the AC grid by its impedance $\underline{\mathbf{Z}}_{\mathrm{G}}$. The feedback interconnection of both systems is given by

$$\underline{\mathbf{G}}_{\mathrm{Z}} = (\mathbf{I} + \underline{\mathbf{Y}}_{\mathrm{H}}\underline{\mathbf{Z}}_{\mathrm{G}})^{-1}\underline{\mathbf{Y}}_{\mathrm{H}} \tag{12}$$

In general, both $\underline{\mathbf{Y}}_{\mathrm{H}}$ and $\underline{\mathbf{Z}}_{\mathrm{G}}$ are fully set 3-by-3 matrices in the natural RST domain, which due to the fact, that converter transformer usually decouples the zero sequence, can be reduced to 2-by-2 matrices in $\alpha\beta$ and respectively in dq domain. This is a special system class of MIMO systems, further referred to as TITO (two inputs two outputs) system, where many problems can be solved analytically and become therewith directly accessible. For HVDC converters, the goal of stability analysis is often to evaluate the influence of a well known converter input admittance to unknown and varying grid impedances, hence stating robustness to control an unknown system.

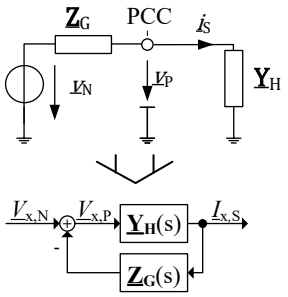

Fig. 4: Control representation of a simplified electrical circuit

4.2 Impedance based stability analysis and their relation to SISO stability theorems

The Nyquist criterion as a frequency domain stability theorem was originally derived for the SISO case and later extended to MIMO systems. As it is well known, its transparent design benefits only hold for the SISO case and much of them are lost during the extension to MIMO systems. Since the Nyquist theorem for the SISO and MIMO case is well known we only refer to e.g. [24–27] for a comprehensive summary, especially for the perquisites on the system transfer function in the MIMO case.

The Nyquist theorem in the SISO case (SNC) directly introduces two measures of robustness, the phase and the gain margin. A stable SISO system is called passive, iff the phase remains between $\pm$ 90°. From the SNC, the conclusion follows, that two passive systems under unity feedback must be stable, independent of the loop gain. The feedback system has infinite gain margin. However, delays in the feedback loop may overcome the limited phase margin and destabilize the system, nonetheless.

The small gain theorem addresses the gain margin and therefore complements the passivity approach. The small gain theorem for the SISO system states, that the feedback connection of two stable SISO systems $\underline{A}$ and $\underline{B}$ is stable, iff $|\underline{A}| \cdot |\underline{B}| < 1 \; \forall \; \omega \in (-\infty, \infty)$. The feedback system has infinite phase margin.

Both concepts establish conditions for so-called structural stability. This means stability is guaranteed as a consequence of the system class (e.g. the class of passive systems). However, model variations often change the system class, since the vast majority of transfer functions only remain passive or fulfill the small gain theorem for a certain range of their parameters and even then only within certain frequency ranges. This observation is very important for the application of passivity theorem-based stability analysis in the HVDC environment since it directly impacts the strength and applicability of the result in real-world applications. The knowledge of structural stability properties and deficiencies of the HVDC input admittance directly leads to boundaries for the AC grid impedance (and vice versa) in which stability and robustness can be guaranteed. E.g., as a consequence of the small gain theorem, if the magnitude of the grid impedance is lower than that of the HVDC within a certain frequency range, the interconnected system cannot become unstable in that range. The same goes for the passivity criterion.

The classical impedance based analysis considers the real part of the converter admittance and demands that

$$\mathbf{Re}\{\underline{Y}_{\mathrm{H}}(\mathrm{j}\omega)\} \geq 0 \; \forall \; \omega \in [-\infty, +\infty] \Leftrightarrow \arg(\underline{Y}_{\mathrm{H}}(\mathrm{j}\omega)) \in [-90^{\circ}, +90^{\circ}], \tag{13}$$

which is equivalent to the converter admittance being passive, given it is stable [16, 26, 28–30]. If the converter admittance is passive in a certain frequency range, where the grid impedance is known with certainty to be passive as well, the system cannot become unstable in that range. However, even a passive converter admittance does not necessarily lead to a stable system, when the AC grid has non-passive regions e.g. because of other actively controlled devices, which is a given at least in the frequency range around the nominal grid frequency. Moreover, condition (13) is very conservative and cannot be fulfilled over the whole frequency range in a real world application control system. It must be ensured, that the

open loop suffices the Nyquist theorem, by adapting the range of allowable phase variations of the grid as well. Instead of purely relying on the passivity of the converter and the grid, mixed boundaries in phase and gain within the framework of the SNC can also be used to achieve less conservative stability conditions.

4.3 MIMO theorems for closed loop stability

The Nyquist theorem in the MIMO case loses two of the main benefits given in the SISO case: First, the clear dependency between open loop transfer functions and the Nyquist curve and secondly the easy definition of the stability and robustness margins. The MIMO Nyquist theorem, also known as generalized Nyquist theorem (GNC)[1, 31, 32], involves the locus of the determinant of the feedback difference matrix (FDM) $\underline{\mathbf{F}} = \mathbf{I} + \underline{\mathbf{G}}_{\mathrm{O}}$ and its correct encirclement of the origin [26, 28]. The definition of the phase and gain margin are no longer meaningful applicable. Due to these facts, the MIMO Nyquist criterion can be used to determine the stability of a given open loop, but not to give robustness measures in terms of phase and gain margins. This is especially disadvantageous, since the robustness for varying grid conditions is an essential design criteria for the HVDC control.

There are equivalents to SISO passivity and small gain theorem for MIMO [25, 33]. However, strict pre-conditions must apply. Moreover, they provide no guarantees about robustness against phase distortions and model parameter variations. Since the grid conditions are mostly only known by statistics and with the rising number of active components, like HVDC and SVC converters, these MIMO theorems are not as useful as in the SISO case.

As stated, MIMO stability criteria have certain drawbacks, when it comes to evaluating the robustness of a certain control system to unknown or varying plants. Therefore, the next section identifies circumstances, under which the MIMO system can be handled by solving adequate multiple SISO problems to restore their benefits and circumvent the design problems introduced by the MIMO criteria.

4.4 Diagonal dominance and it's application to the GNC

In this section the concept of generalized diagonal dominance (GDD) is introduced. This concept belongs to the so-called direct Nyquist array methods. The common idea of these concepts is the reduction of the MIMO problem into multiple SISO problems, which can be solved with the classical SISO open-loop shaping methods. Therefore, this methodology is called a quasi-classical approach and dates back to the 1970th with the works of MacFarlane and Rosenbrock [24].

The GNC problem is stated as the locus of the determinant of the FDM, which can also be given by the eigenvalues of this matrix:

$$\det(\underline{\mathbf{F}}) = \det(\mathbf{I} + \underline{\mathbf{G}}_{\mathrm{O}}) = \prod_{i}^{n} \lambda_i(\underline{\mathbf{F}}) = \prod_{i}^{n} (1 + \lambda_i(\underline{\mathbf{G}}_{\mathrm{O}})) \tag{14}$$

With Eq.(14) the MIMO problem is already decomposed into n SISO problems, for TITO system $n = 2$. Since the grid impedance is mostly unknown, the loci of the eigenvalues of $\underline{\mathbf{G}}_{\mathrm{O}} = \underline{\mathbf{Y}}_{\mathrm{C}}\underline{\mathbf{Z}}_{\mathrm{G}}$ as a function of $\mathrm{j}\omega$ cannot be exactly calculated. However, the eigenvalues of a TFM can be approximated by the main diagonal elements, if that matrix is diagonal dominant (DD) or generalized diagonal dominant (GDD).

A matrix $\underline{\mathbf{A}} \in \mathbb{C}^{n \times n}$ is DD if it is row or column dominant, meaning

$$\forall i : |\underline{a}_{ii}| > \sum_{j;j\neq i}^{n} |\underline{a}_{ji}| \quad \text{or} \quad \forall i : |\underline{a}_{ii}| > \sum_{j;j\neq i}^{n} |\underline{a}_{ij}|. \tag{15}$$

This translates to the easy condition in the TITO case, that the absolute value of each diagonal element has to be greater than the absolute value of its related row or column off-diagonal element $\forall\, \omega \in (-\infty, \infty)$. The Gershgorin theorem now assures, that the eigenvalues of $\underline{\mathbf{A}}$ rest within circles given by the midpoint $\underline{a}_{ii}$ and radii given by $\sum_{j;j\neq i}^{n} |\underline{a}_{ji}$ or $\sum_{j;j\neq i}^{n} |\underline{a}_{ij}|$ for row- or column dominance, respectively. As one can easily see, the approximations exclude the origin of the complex plane and therefore the continuous change in phase of the loci of the eigenvalues and of the diagonal elements are the same. Hence, the diagonal elements are a sufficient approximation for the GNC criterion.

A matrix $\underline{\mathbf{A}} \in \mathbb{C}^{n \times n}$; $\underline{\mathbf{A}}$ irreducible, is GDD if there is an invertible (and hence non-singular) diagonal transformation matrix $\underline{\mathbf{R}}$ such that $\tilde{\underline{\mathbf{A}}} := \underline{\mathbf{R}} \cdot \underline{\mathbf{A}} \cdot \tilde{\underline{\mathbf{R}}}$ is DD. The similarity transformation with a diagonal matrix ensures, that the eigenvalues AND the diagonal elements of $\underline{\mathbf{A}}$ and $\tilde{\underline{\mathbf{A}}}$ are the same. Therefore, the

transformation only affects the radii of the Gershgorin bounds. Hence, it follows immediately, the GDD criterion is less restrictive than the DD criterion. Nonetheless, both conditions imply that the Gershgorin bounds do not include the origin and therefore are equivalent in terms of the application to the GNC.

The matrix $\underline{\mathbf{A}}$ is GDD iff $\lambda_\mathrm{P}\{\mathbf{C}(\underline{\mathbf{A}})\} < 1$, where λ_P denotes the Perron-Root of

$$\mathbf{C}(\underline{\mathbf{A}}) := \mathrm{diag}\left(\frac{1}{|\underline{a}_{ii}|}\right) \cdot \begin{bmatrix} 0 & |\underline{a}_{12}| & \dots & |\underline{a}_{1n}| \\ |\underline{a}_{21}| & 0 & \dots & |\underline{a}_{2n}| \\ \vdots & \vdots & \ddots & \vdots \\ |\underline{a}_{n1}| & |\underline{a}_{n2}| & \dots & 0 \end{bmatrix}. \tag{16}$$

The Gershgorin theorem can also be stated in relation to the Perron-Root $\lambda_\mathrm{P}\{\mathbf{C}(\underline{\mathbf{A}})\}$ with $|\underline{a}_{ii}| \cdot \lambda_\mathrm{P}$ as bounds for the Gershgorin circles. This also shows directly, that the bound does not include the origin. The condition that $\underline{\mathbf{A}}$ is irreducible implies that the matrix $\mathbf{C}$ is also irreducible, then since $\mathbf{C}$ is positive real by construction and irreducible by assumption, the Perron-Frobenius theorem ensures the existence of the Perron-Root. For TITO systems the assumption that $\underline{\mathbf{A}}$ is irreducible is not necessary since if $\underline{\mathbf{A}}$ is reducible, it is of triangular form and the eigenvalues are give directly by the main diagonal elements. GDD is sufficient to justify SISO stability analysis. However, in frequency ranges where the Perron-Root is close to one, robustness criteria like phase and gain margin might fail.

4.5 Requirements to the grid impedance to ensure the validity of SISO stability analysis

In the previous section conditions to the FDM, DD and GDD, have been derived, that would allow the common SISO approach (e.g.[5–7, 13–15]) for converter $\leftrightarrow$ grid stability analysis. That approach is only valid iff the feedback difference is DD or GDD. In the next chapter it will be shown, that the converter input admittance, by itself is never DD or GDD for the whole frequency range, hence there are boundaries to the grid impedance that have to be met, to ensure DD or GDD for the FDM and to be able to use SISO criteria to investigate system stability.

During project execution, the grid impedance is often given from transmission system operators to the vendor for a set of frequencies as polygons in the complex plain where the grid impedance most like would rest during converter runtime. Hence, the exact impedance is unknown and stability and interactions have to be investigated based on the converter input impedance alone. For that, two assumptions are crucial: the grid impedance is symmetrical (hence, diagonal and identical in the $\alpha\beta$ frame) and passive. These precondition seem restrictive, are however reasonable for high voltage AC grids. In addition, from the previous section another limitation arises: The FDM must be diagonal dominant.

The converter admittance can only be calculated in a dq frame and cannot be transferred to $\alpha\beta$ without losing its LTI property, due to lack of skew symmetry. In Section 3 is also shown, that a diagonal and identical $\alpha\beta$ frame grid system matrix is fully coupled in the dq frame, with a maximum coupling in the frequency range below 50 Hz. Since its specific values are unknown, diagonal dominance cannot be ensured. Hence, this would not be usable for a SISO investigation. However, transferred in the dq_PN frame, the grid impedance matrix is diagonal again. This operation is also possible on the given impedance polygons since it is a simple frequency shift from the $\alpha\beta$ frame (see Eq.(10)).

The requirement for GDD for a given converter input admittance and a grid impedance, only known by its structural properties in the dq_PN frame denotes to:

$$\underline{\mathbf{F}}^{\mathrm{dq}}_{\mathrm{PN}} = \mathbf{I} + \underline{\mathbf{Y}}^{\mathrm{dq}}_{\mathrm{C,PN}} \underline{\mathbf{Z}}^{\mathrm{dq}}_{\mathrm{G,PN}} = \begin{bmatrix} 1 + \underline{Y}^{\mathrm{dq}}_{\mathrm{C,PP}} \underline{Z}^{\mathrm{dq}}_{\mathrm{G,PP}} & \underline{Y}^{\mathrm{dq}}_{\mathrm{C,PN}} \underline{Z}^{\mathrm{dq}}_{\mathrm{G,NN}} \\ \underline{Y}^{\mathrm{dq}}_{\mathrm{C,NP}} \underline{Z}^{\mathrm{dq}}_{\mathrm{G,PP}} & 1 + \underline{Y}^{\mathrm{dq}}_{\mathrm{C,NN}} \underline{Z}^{\mathrm{dq}}_{\mathrm{G,NN}} \end{bmatrix} \tag{17}$$

$$\lambda_\mathrm{P}\{\mathbf{C}(\underline{\mathbf{F}}^{\mathrm{dq}}_{\mathrm{PN}})\} = \sqrt{\frac{|\underline{Y}^{\mathrm{dq}}_{\mathrm{C,PN}} \underline{Z}^{\mathrm{dq}}_{\mathrm{G,NN}}|}{|1 + \underline{Y}^{\mathrm{dq}}_{\mathrm{C,PP}} \underline{Z}^{\mathrm{dq}}_{\mathrm{G,PP}}|} \cdot \frac{|\underline{Y}^{\mathrm{dq}}_{\mathrm{C,NP}} \underline{Z}^{\mathrm{dq}}_{\mathrm{G,PP}}|}{|1 + \underline{Y}^{\mathrm{dq}}_{\mathrm{C,NN}} \underline{Z}^{\mathrm{dq}}_{\mathrm{G,NN}}|}} \overset{!}{<} 1 \tag{18}$$

With a conservative approximation, that condition (18) is fulfilled, if either fraction is less than 1, direct boundaries for $\underline{Z}_{\mathrm{G,PP}}$ and $\underline{Z}_{\mathrm{G,NN}}$ can be derived.

$$|\underline{Z}_{\mathrm{G},ii}| \overset{!}{<} \min\left(1/\left(-|\underline{Y}_{\mathrm{H},ii}|\cos\Sigma\varphi \pm \sqrt{|\underline{Y}_{\mathrm{H,od}}|^2 - |\underline{Y}_{\mathrm{H},ii}|^2 \sin^2\Sigma\varphi}\right)\right) \quad i \in \{\mathrm{P},\mathrm{N}\},\ \Sigma\varphi \in [-\pi,\pi],\ \forall \mathrm{j}\omega$$
$$\text{where } \Sigma\varphi = \arg(\underline{Y}_{\mathrm{H},ii}) + \arg(\underline{Z}_{\mathrm{G},ii}) \text{ and } \underline{Y}_{\mathrm{H,od}} \text{ is the off-diagonal element of line or column } i \tag{19}$$

If the condition of Eq.(19) is fulfilled for either both lines or both columns, the system is GDD and stability can be analyzed using the common SISO tools and if the condition of Eq.(19) is fulfilled with enough margin, even the SISO robustness criteria, like phase and gain margin, are valid. Otherwise, the evaluation of the MIMO GNC is necessary. Hence, the condition of Eq.(19) can be used to indicate areas of the given grid impedance polygons where SISO analysis is possible and areas where the SISO approach is not valid.

5 Properties of and requirements to the converter input impedance as well as the underlying control design

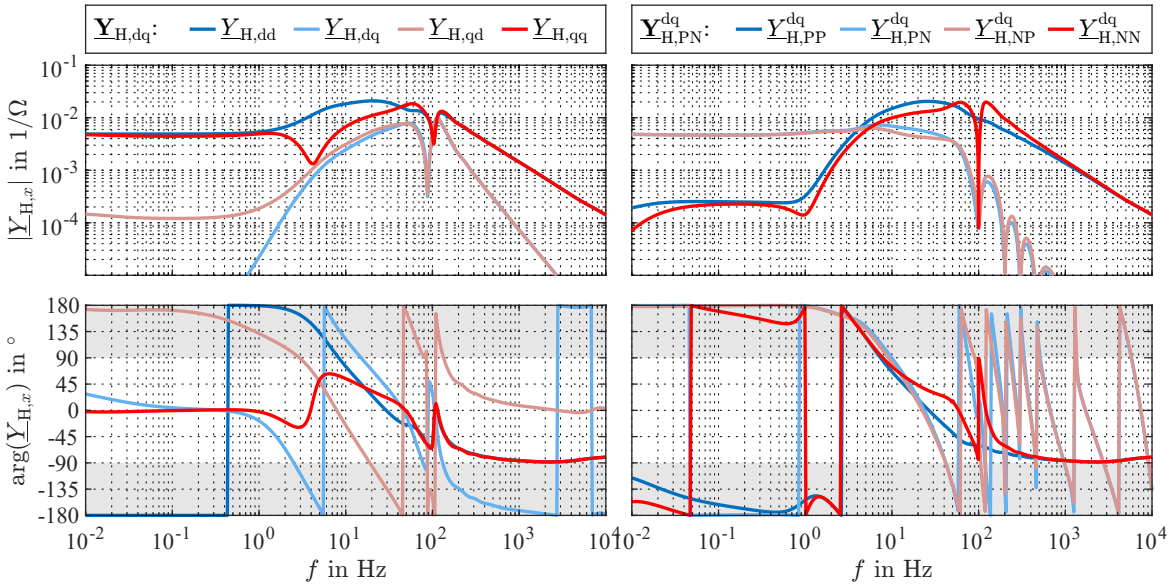

Fig. 5: Calculated input admittance in a dq (left) and a dq_{PN} (right) frame for maximum power rectifier operation

In this section, the findings of the previous sections are brought together on an exemplary converter input admittance, calculated according to Section 2. Fig. 5 shows the converter input admittance in the dq and the dq_{PN} coordinate system.

For $f < 80\,\mathrm{Hz}$ the converter input admittance is highly operation point dependent. While the admittance itself shows strong diagonal dominance in dq below 90 Hz and above 200 Hz, the admittance in dq_{PN} shows strong diagonal dominance above 10 Hz, with an exception at 100 Hz, and no diagonal dominance below. The main diagonal admittance in both frames is passive above 10 Hz. It is noteworthy, that for the higher frequencies, this is mainly because of the real part of the converter transformer impedance. Due to unavoidable dead times, the control impedance can never be passive at higher frequencies. Hence, to avoid negative damping in this area, the controller proportional gain must be significantly smaller than the real part of the transformer impedance. This is especially challenging with transformers optimized for their losses.

The negative damping area in the low frequency range of the converter input admittance is directly given by the bandwidth of the controllers integral parts. Any conventional control system containing integrators shows this behavior. The higher the dynamic of these controllers, the higher is the crossover frequency, where the real part of the control impedance becomes positive. Hence, the requirement for a passive converter input impedance is diametral to its performance requirements (compare to [14–16]).

The coupling between the PPS and the NPS is mainly a result of the separated active (energy) and reactive power control loops as well as the PLL dynamics, since e.g. any oscillation in the energy system in combination with the Park transformation directly convolves to a PPS and NPS response. This could only be mitigated by a strong limitation of the bandwidth of these controllers as well as the PLL, which again is diametral to their performance requirements.

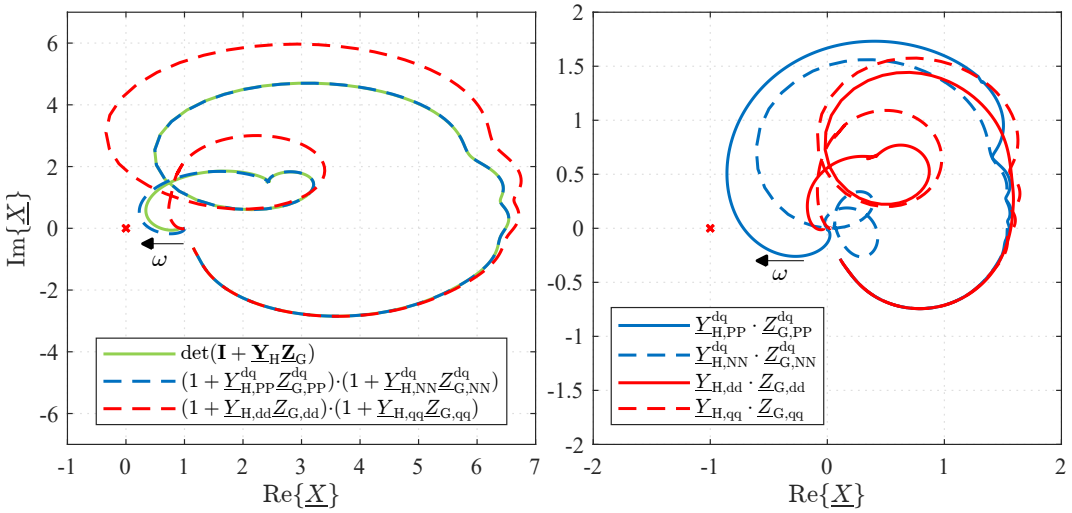

(a) locus of the FDM determinant (GNC) vs. the approximated eigenvalues from the main diagonal elements in dq and dq_{PN}

(b) loci of main diagonal open loop transfer functions for a classical SISO interpretation in dq and dq_{PN}

Fig. 6: Comparison of the evaluation of the eigenvalue locus according to the MIMO GNC with the approximated loci of the eigenvalues by the main diagonal elements of the FDM containing a thevenin source grid impedance for a short circuit level of 3 GVA

Fig. 6a shows the GNC locus evaluated for the full FDM in comparison to its approximation by the diagonal elements in the dq and dq_{PN} frame. The deviation between the GNC locus and the approximated loci provides a measure for the quality of the approximation. Due to the strong coupling of the grid impedance between the d and q axis in the dq frame the approximation of the FDM by its main diagonal elements is insufficient, especially for lower frequencies. Evaluation of stability margins would be way too optimistic in that frame as shown in Fig. 6b. In the dq_{PN} frame, the eigenvalue approximation is a near perfect fit to the locus of the FDM GNC. While *PN* transformation does not affect the eigenvalues of the FDM, its positive influence on the diagonal dominance becomes obvious. Hence, the main diagonal elements in the dq_{PN} frame are suitable for SISO stability and robustness investigation.

Fig. 7 shows the evaluation of Eq.(19) for the dq_{PN} converter input admittance shown in Fig. 5. In addition, for each main diagonal element, the nominal thevenin grid impedance in dq_{PN} for a short circuit level of 3 GVA is plotted as a reference. Eq.(19) gives an upper bound for the magnitude of each main diagonal element of the grid impedance in the dq_{PN} frame, within which the requirement for GDD is fulfilled. Obviously, a smaller Perron-Root implies a stronger GDD property, since possible deviations between the GNC locus and its approximation are bounded narrower, which improves the validity of

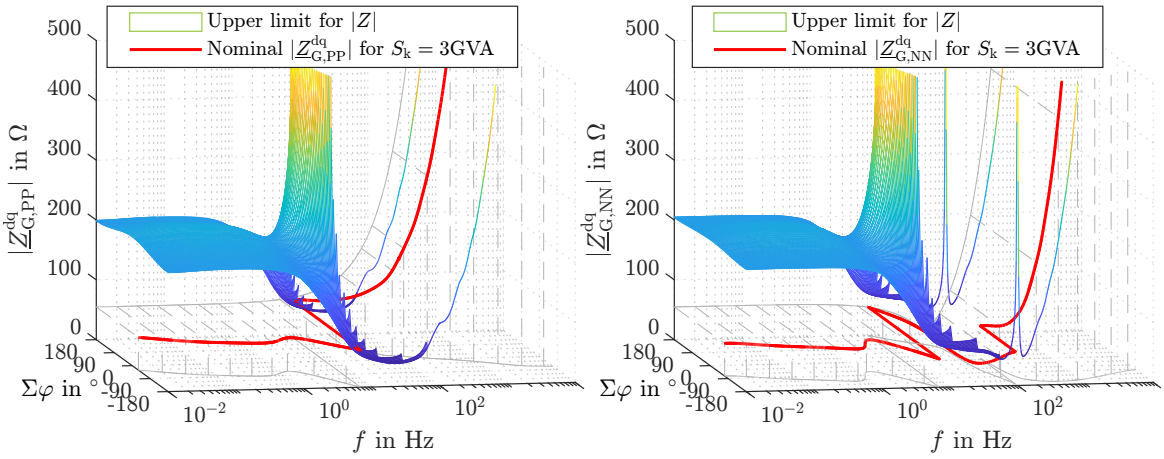

Fig. 7: Upper bounds of the grid impedance for the converter admittance of Fig. 5 and comparison to a nominal grid impedance at a short circuit level of 3 GVA

SISO open loop investigations. The surface given by Eq.(19) opens for frequencies above approximately 10 Hz, meaning that there is no limit to the magnitude of the grid impedance in that area. Only where the summarized angle of $\underline{Y}^{\mathrm{dq}}_{\mathrm{C,PP/NN}}$ and $\underline{Z}^{\mathrm{dq}}_{\mathrm{G,PP/NN}}$ is close to $\pm 180^{\circ}$, hence at the passivity limit of the feedback system, there is still an upper bound. In that frequency range the coupling between the axis of the converter input admittance is very low (in all reference frames) and the restrictions on the system class of the AC grid impedance could be weakened.

Since Fig. 7 shows only the evaluation for each fraction of Eq.(19), it seems that GDD is violated for $|\underline{Z}^{\mathrm{dq}}_{\mathrm{G,PP}}|$ between 6 and 8 Hz. However, since the product of both fractions must be less than 1, only DD is violated while the requirements for GDD are still met with the nominal grid impedance.

For the given example control and configuration, in the frequency range up to about 10 Hz SISO stability investigation is only valid up to a grid impedance magnitude of about 200 Ω. Obviously any grid resonance in that frequency range would exceed this limit. Hence, very detailed models and most likely a MIMO GNC investigation are necessary, for e.g. sub-synchronous torsion interaction and power oscillation damping investigations.

6 Conclusion

Ensuring robust stability when installing a new HVDC station to the AC grid is a fundamental design criterion. The commonly used approach for this investigation is based on the SISO Nyquist theorem, considering only the main diagonal elements of the converter input admittance to draw conclusions on the stability margins for the interconnected feedback system with the AC grid. This is clearly motivated by the obvious robustness criteria given by the SISO Nyquist theorem. In this paper, a control theoretical foundation for the validity of this SISO approach has been derived. At first by showing the limitations to the linearity of reference system transformations and the limitations of the SISO approach applied to MIMO systems, due to the cross coupling between e.g. the d- and q-axis within the converter admittance. By introducing the MIMO criteria for diagonal dominance and more important generalized diagonal dominance, a comprehensive and sufficient boundary can be drawn, separating systems classes, where a SISO investigation is justified and where a MIMO stability analysis via the GNC is advisable. This requires knowledge from both, the converter and the AC grid system. Based on that, it has been shown, that this criterion can only be implemented for a certain class of AC systems, namely passive, symmetrical systems where the α and β grid impedance components are identical. A symmetrical AC grid in the αβ-frame is diagonal in the dq_{PN} frame, allowing the assessment of GDD solely based on the structural properties of the converter input admittance. Passivity of the AC system is a necessary condition to enable stability evaluation via the phase margin of the converter input admittance.

With a generic converter control system with only basic control loops for converter current, energy and reactive power an exemplary converter input impedance was calculated. Based on that, it has been demonstrated, that a SISO robustness investigation based on the main diagonal elements of the converter admittance in the dq frame is most likely insufficient due to the strong coupling in the grid impedance in that frame. However, in the dq_{PN} frame, the systems eigenvalues can be matched with good accuracy by the main diagonal elements, as long as the criteria for GDD are fulfilled. Based on the calculated converter input admittance exact boundaries to the grid impedance magnitude can be derived. Within these boundaries, stability and robustness investigation based on the SISO Nyquist theorem is justified. It has been shown, that especially in the high frequency range due to strong diagonal dominance in the converter admittance the validity of SISO robustness investigation can be ensured. However, in the low frequency range careful evaluation of and especially a deeper knowledge on the grid impedance is necessary to evaluate robustness.

References

[1] L. Harnefors. “Modeling of Three-Phase Dynamic Systems Using Complex Transfer Functions and Transfer Matrices”. In: *IEEE Transactions on Industrial Electronics* 54.4 (2007), pp. 2239–2248.

[2] Y. A. Familiant, J. Huang, K. A. Corzine, et al. “New Techniques for Measuring Impedance Characteristics of Three-Phase AC Power Systems”. In: *IEEE Transactions on Power Electronics* 24.7 (2009), pp. 1802–1810.

[3] G. Francis, R. Burgos, D. Boroyevich, et al. “An algorithm and implementation system for measuring impedance in the D-Q domain”. In: *IEEE Energy Conversion Congress and Exposition*. 2011, pp. 3221–3228.

[4] R. Turner, S. Walton, and R. Duke. “A Case Study on the Application of the Nyquist Stability Criterion as Applied to Interconnected Loads and Sources on Grids”. In: *IEEE Transactions on Industrial Electronics* 60.7 (2013), pp. 2740–2749.

[5] M. Cespedes and J. Sun. “Impedance Modeling and Analysis of Grid-Connected Voltage-Source Converters”. In: *IEEE Transactions on Power Electronics* 29.3 (2014), pp. 1254–1261.

[6] X. Wang, F. Blaabjerg, and W. Wu. “Modeling and Analysis of Harmonic Stability in an AC Power-Electronics-Based Power System”. In: *IEEE Transactions on Power Electronics* 29.12 (2014), pp. 6421–6432.

[7] B. Wen, D. Dong, D. Boroyevich, et al. “Impedance-Based Analysis of Grid-Synchronization Stability for Three-Phase Paralleled Converters”. In: *IEEE Transactions on Power Electronics* 31.1 (2016), pp. 26–38.

[8] I. Vieto and J. Sun. “Sequence Impedance Modeling and Converter-Grid Resonance Analysis Considering DC Bus Dynamics and Mirrored Harmonics”. In: *2018 IEEE 19th Workshop on Control and Modeling for Power Electronics (COMPEL)*. 2018, pp. 1–8.

[9] X. Wang, L. Harnefors, and F. Blaabjerg. “Unified Impedance Model of Grid-Connected Voltage-Source Converters”. In: *IEEE Transactions on Power Electronics* 33.2 (2018), pp. 1775–1787.

[10] C.M. Wildrick, F.C. Lee, B.H. Cho, et al. “A method of defining the load impedance specification for a stable distributed power system”. In: *IEEE Transactions on Power Electronics* 10.3 (1995), pp. 280–285.

[11] H. Saad, Y. Fillion, S. Deschanvres, et al. “On Resonances and Harmonics in HVDC-MMC Station Connected to AC Grid”. In: *IEEE Transactions on Power Delivery* 32.3 (2017), pp. 1565–1573.

[12] Cigré WG B4.67. “AC side harmonics and appropriate limits for VSC HVDC”. In: *Techn. Brochure 754* (2019).

[13] H. Zhang, L. Harnefors, X. Wang, et al. “Stability Analysis of Grid-Connected Voltage-Source Converters Using SISO Modeling”. In: *IEEE Transactions on Power Electronics* 34.8 (2019), pp. 8104–8117.

[14] C. Hirsching, S. Wenig, S. Beckler, et al. “Passivity-Based Sensitivity Analysis of the Inner Current Controller in Grid-Following MMC-HVdc Applications - An Overview”. In: *IECON 2020 The 46th Annual Conference of the IEEE Industrial Electronics Society*. 2020, pp. 1412–1417.

[15] C. Hirsching, A. Bisseling, S. Wenig, et al. “On the impact of controller implementations on passivity and damping properties in grid-following MMC-HVdc applications”. In: *accepted for the 47th Annual Conference of the IEEE Industrial Electronics Society*. 2021.

[16] L. Harnefors, M. Bongiorno, and S. Lundberg. “Input-Admittance Calculation and Shaping for Controlled Voltage-Source Converters”. In: *IEEE Transactions on Industrial Electronics* 54.6 (2007), pp. 3323–3334.

[17] A. Bayo-Salas, J. Beerten, J. Rimez, et al. “Impedance-based stability assessment of parallel VSC HVDC grid connections”. In: *11th IET International Conference on AC & DC Power Transmission*. 2015, pp. 1–9.

[18] A. Rygg, M. Molinas, C. Zhang, et al. “A Modified Sequence-Domain Impedance Definition and Its Equivalence to the dq-Domain Impedance Definition for the Stability Analysis of AC Power Electronic Systems”. In: *IEEE Journal of Emerging and Selected Topics in Power Electronics* 4.4 (2016), pp. 1383–1396.

[19] G. Herold. *Drehstromsysteme, Leistungen, Wirtschaftlichkeit*. 3rd ed. Vol. 1. Elektrische Energieversorgung. Wilburgstetten: J. Schlembach, 2011.

[20] D.N. Zmood, D.G. Holmes, and G.H. Bode. “Frequency-domain analysis of three-phase linear current regulators”. In: *IEEE Transactions on Industry Applications* 37.2 (2001), pp. 601–610.

[21] J. Sun. “Small-Signal Methods for AC Distributed Power Systems–A Review”. In: *IEEE Transactions on Power Electronics* 24.11 (2009), pp. 2545–2554.

[22] A. Rygg, M. Molinas, C. Zhang, et al. “On the Equivalence and Impact on Stability of Impedance Modeling of Power Electronic Converters in Different Domains”. In: *IEEE Journal of Emerging and Selected Topics in Power Electronics* 5.4 (2017), pp. 1444–1454.

[23] C. Zhang, X. Cai, A. Rygg, et al. “Sequence Domain SISO Equivalent Models of a Grid-Tied Voltage Source Converter System for Small-Signal Stability Analysis”. In: *IEEE Transactions on Energy Conversion* 33.2 (2018), pp. 741–749.

[24] J. Raisch. *Mehrgrössenregelung im Frequenzbereich*. Methoden der Regelungs- und Automatisierungstechnik. Oldenbourg Wissenschaftsverlag, 1994.

[25] B. Brogliato, R. Lozano, B. Maschke, et al. *Dissipative systems analysis and control*. en. 2nd ed. Communications and Control Engineering Series. London, England: Springer, 2007.

[26] J. Lunze. *Regelungstechnik 2 Mehrgrößensysteme, Digitale Regelung*. 8th ed. Springer, 2014.

[27] J. Sun. “Impedance-Based Stability Criterion for Grid-Connected Inverters”. In: *IEEE Transactions on Power Electronics* 26.11 (2011), pp. 3075–3078.

[28] H. Unbehauen. *Regelungstechnik I*. 15th ed. Wiesbaden: Vieweg + Teubner, 2008.

[29] L. Harnefors, X. Wang, A. G. Yepes, et al. “Passivity-Based Stability Assessment of Grid-Connected VSCs — An Overview”. In: *IEEE Journal of Emerging and Selected Topics in Power Electronics* 4.1 (2016), pp. 116–125.

[30] A. J. Agbemuko, J. L. Domínguez-García, O. Gomis-Bellmunt, et al. “Passivity-Based Analysis and Performance Enhancement of a Vector Controlled VSC Connected to a Weak AC Grid”. In: *IEEE Transactions on Power Delivery* 36.1 (2021), pp. 156–167.

[31] C. Desoer and Y.-T. Wang. “On the generalized nyquist stability criterion”. In: *IEEE Transactions on Automatic Control* 25.2 (1980), pp. 187–196.

[32] J. Samanes, A. Urtasun, E. L. Barrios, et al. “Control Design and Stability Analysis of Power Converters: The MIMO Generalized Bode Criterion”. In: *IEEE Journal of Emerging and Selected Topics in Power Electronics* 8.2 (2020), pp. 1880–1893.

[33] S. Skogestad and I. Postlethwaite. *Multivariable feedback control*. Chichester, England: John Wiley & Sons, 1996.